Identification of snow cover regimes through spatial and temporal clustering of satellite microwave brightness temperatures

C.J.Q. Farmer [a,*], T.A. Nelson [a], M.A. Wulder [b], C. Derksen [c]

[a] Spatial Pattern Analysis & Research Laboratory, University of Victoria, Department of Geography, Victoria, British Columbia, Canada
[b] Canadian Forest Service, Pacific Forestry Center, Natural Resources Canada, Victoria, British Columbia, Canada V8Z 1 M5
[c] Environment Canada, Atmospheric Science and Technology Directorate, Climate Research Division, Climate Processes Section, Downsview, Ontario, Canada M3H 5 T4

ARTICLE INFO

ABSTRACT

Areas of similar ecology are often delineated based on homogenous topography, temperature, and land cover. Once delineated, these zones become the basis for a wide variety of scientific research and management activities. For instance, in Canada, ecozones are commonly utilized ecological management units delineated using geographic, topographic, and climatic information aided by spring and summer vegetation conditions. Snow cover has an influence on local and regional hydrological conditions and climate, as well as on animal habitats. As such, we posit that inclusion of winter conditions, incorporating spatial- and temporal-variation in snow cover is an additional element for consideration when delineating areas with homogenous conditions. In our analysis we use satellite passive microwave brightness temperatures from 19 years of Special Sensor Microwave/Imager (SSM/I) measurements to produce a daily time-series on snow cover, and demonstrate how these data can be used to delineate areas of similar winter conditions. We use splines and curve fitting to generalize the dense time-series (of over 6900 days) to a set of metrics, and select three for use in cluster-based generalization of snow cover regimes: annual maximum difference between 37 and 19 GHz SSM/I measurements (with differences in magnitudes indicative of snow accumulation), variation of 37–19 GHz brightness temperatures (indicative of snow cover variability), and variation in the rate of brightness temperature change during the snow melt season (indicative of seasonal change). Our results indicate that these metrics produce spatial units that are unique, and not captured by conventional ecological management units, while also producing spatial units that cohere to those generated from summer conditions. Spatial units that are found to have spatial cohesion between summer and winter data sources are located in regions where the amount of snow tends to be low, and snow cover variability minimal. We propose that snow cover regimes may be used to augment typical vegetation-based ecological zonations or to provide insights on hydrology and animal habitat conditions. Inclusion of winter conditions is especially important when areal delineations are used to monitor impacts of climate change, and as a baseline for monitoring changes in snow cover amount, extent, and/or distribution.

© 2009 Elsevier Inc. All rights reserved.

1. Introduction

Ecological management units organize knowledge and generalize complex interrelationships, providing a means to identify geographic regions with similar properties (Hirsch et al., 1978). Such geographic regions tend to respond similarly to disturbances and pressures, and by defining ecological management units it is possible to generalize knowledge regarding the spatial and temporal processes affecting a region (Hirsch et al., 1978). Ecological management units thus aid in the description, characterization, and delineation of physical processes necessary for scientific modeling, management, and conservation of ecosystems (Blasi et al., 2000; Sims et al., 1996). As well, ecological

management units are essential for extrapolating research results from single locations to larger areas.

In Canada, standard ecological units are based largely on spring and summer landscape conditions (e.g. Rowe & Sheard, 1981; Wiken, 1986; Ironside, 1991). Temporally, it is often the spring green-up and fall senescence that are used for characterizing land cover at both regional (e.g. Moody & Johnson, 2001) and global scales (e.g. Moulin et al., 1997; DeFries et al., 1995; Justice et al., 1985). This may be problematic for understanding the interactions of winter-controlled processes, such as spring snow melt and runoff, or for regions where a substantial portion of the year is spent covered with snow. Terrestrial snow cover has a significant influence on global and regional climate (Barnett et al., 2005; Derksen et al., 1998a), the hydrologic cycle (Serreze et al., 2000; Derksen et al., 2000a,b; Wulder et al., 2007) and local snow melt release (Luce et al., 1998). While appropriate for many applications, the current suite of ecological management units in Canada does not consider winter season

characteristics. International standards and practices for ecological zonation, as currently implemented, may not sufficiently capture Canadian ecological conditions. The current ecological zonation for Canada is meeting operational and reporting needs, but consideration may be given to possible improvements or data sources that incorporate unique Canadian conditions to augment the established management units.

Spatial and temporal patterns of snow water equivalent (SWE) accumulation, evolution, and melt influence the spatial and temporal patterns and processes of many ecological systems. For example, the spatial distribution of snow impacts meso-scale processes of biological systems in arctic and alpine ecosystems (Walker et al., 1993, 1999). As well, spatial–temporal patterns of SWE influence biodiversity (Duro et al., 2007), species and community distributions (Walker et al., 1999), and anthropogenic processes such as tourism, recreation, and urban and agricultural water supply (Walker et al., 1993). Analyzing regional variations in the spatial–temporal patterns of SWE will highlight unique regimes, or groups of locations with similar spatial and temporal characteristics. SWE regimes are useful for assessing the impact of snow cover and SWE on abiotic and biotic systems within a region and, like ecological units, provide a mechanism for extrapolating winter processes observed at specific locations to landscapes. The goals of this paper are to examine the long-term temporal characteristics of SWE as expressed by satellite passive microwave brightness temperatures (Tb), and identify if and how they vary across the landscape in order to delineate geographically distinct SWE regimes. These regimes can then be used to partition the landscape into winter-based management zones, to be compared with current spring and summer based ecological management units. These goals will be addressed through the following primary objectives:

1. to apply an advanced curve fitting procedure, which takes into account features and fluctuations in the dataset, to a temporal sequence of passive microwave Tb's,
2. to derive annual and inter-annual temporal metrics of Tb variations through time, based on the fitted curve,
3. to delineate geographically distinct winter-based management zones by clustering temporal metrics generated for local regions within the study area, and
4. to examine the variability of winter conditions derived from the Tb regimes within current spring and summer ecological management units.

We limit our analysis to the SSM/I satellite record, which provides continuous daily satellite data records for North America since July 1987. Due to the inherent characteristics of space-borne passive microwave data, such as all-weather imaging, frequent overpass times, sensitivity of specific measurement frequencies to snow pack volume scatter, and an existing long-term data record validated for the planar regions of Canada (Derksen et al., 2002, 2005; Sokol et al., 2003; Derksen et al., 2000a,b), these datasets are appropriate for SWE regime characterization. Through capitalization upon the continuous spatial coverage, and fine temporal resolutions of current passive microwave derived SWE datasets, this research provides insight not accessible by conventional space–time SWE research which has emphasized spatial trends of snow cover and SWE over short time periods (e.g. Derksen et al., 1998b,c), or coarse-scale spatial trends (i.e. regional analysis) of snow cover and SWE over longer time periods (e.g. Brown, 2000; Laternser & Schneebeli, 2003).

2. Study area and data

2.1. Deriving SWE from passive microwave radiometry

Over the past two decades, SWE datasets have been developed using passive microwave radiometry at regional (Derksen et al., 2000a,b; Derksen & McKay, 2006; Walker & Goodison, 2000) and hemispheric scales (Tait, 1996; Pulliainen & Halliskainen, 2001; Grody & Basist, 1996). These datasets have largely been the result of algorithm developments for Scanning Multichannel Microwave Radiometer (SMMR; 1978–1987), and Special Sensor Microwave/Imager (SSM/I; 1987–present) data, and have been used for research on the interaction between snow cover and climate (Derksen et al., 2000a,b), as well as validation of regional climate models (MacKay et al., 2003). Theoretical estimation of SWE from passive microwave radiometry is primarily a function of the interaction of snow crystals with the microwave radiation naturally emitted by the earth, and assumes that as the depth and density of snow increases, scattering of the passive microwave signal also increases (Foster et al., 1999). In general, shorter wavelength energy (i.e. 37 GHz) is more readily scattered by crystals in the snow pack than longer wavelength energy (i.e. 19 GHz), allowing the difference between these two satellite measured frequencies to be used to estimate SWE (Foster et al., 1999; Walker & Goodison, 2000; Chang et al., 2003). In regions where interactions between the atmosphere, snow cover, and the underlying ground surface are complex, such as mountainous regions, or regions with dense forest cover, complications may arise in the estimation of SWE from passive microwave data (Tait, 1996; Pulliainen & Halliskainen, 2001; Foster et al., 1999). These challenges arise from a range of physical parameters including the underlying land cover, topography, and overlying vegetation. In addition, issues such as snow wetness, snow crystal size, depth hoar, and ice crusts may cause complications in interpreting the passive microwave signatures (Derksen et al., 2000a,b).

Despite these challenges, SWE estimates with vertical accuracies of as low as ±15 mm across a single pixel have been obtained from passive microwave radiometry in many of the low-relief regions of Central Canada (Derksen et al., 2003, 2005), where low forest cover, typically dry snow conditions during winter, and a lack of complex underlying topography make relationships between SWE and Tbs relatively straightforward (Goodison & Walker, 1995). In general, algorithm development for SWE retrieval from space-borne passive microwave Tbs in Canada has focused on the open prairie and boreal forest regions of central Canada (Goodison & Walker, 1995; Walker & Goodison, 2000; Goita et al., 2003). Assessments of algorithm performance in these areas have shown that retrievals are suitable for large-area climatological analysis (Derksen et al., 2003a,b), though systematic SWE underestimation remains a problem in mountainous and densely vegetated areas (Derksen et al., 2003; Walker & Silis, 2002).

2.2. Study area and data

This study will be constrained to the Canadian prairies (Fig. 1), extending from approximately −120° to −90° West, and from 50° to 60° North. We use daily Tb (in Kelvin) from the SSM/I passive microwave radiometer on-board the Defense Meteorological Satellite Program (DMSP) F8, F11 and F13 satellites in the 25 km Equal Area Scalable Earth Grid (EASE-Grid) format (see Armstrong & Brodzik, 1995) acquired from the National Snow and Ice Data Center (Knowles et al., 1999; Armstrong et al., 2002). The difference between the 37 and 19 GHz vertically polarized channels was calculated, and in all cases, data collected during the morning overpass (approximately 0600 local time) were used for analysis to reduce errors induced by afternoon snow melt (Derksen et al., 2000a,b). The 37 and 19 GHz vertically polarized channels are the conventional frequencies used to estimate SWE in most algorithms (Goodison, 1989). As such, we chose to utilize Tb difference (37–19 GHz) instead of SWE values retrieved using the Environment Canada suite of algorithms (Goodison & Walker, 1995; Goita et al., 2003) in order to remove one layer of data processing, and directly apply the statistical techniques to the satellite measurements. All the Environment Canada SWE algorithms are linear equations, so the Tb difference is a direct proxy for SWE: a larger difference represents greater SWE. In areas where algorithm confidence is high (i.e. the prairies) interpretation of the SWE

Fig. 1. Study region encompasses the Canadian prairies, extending from approximately −120° to −90° West, and from 60° to 50° North, and an area of over 2.5×10^6 km².

retrievals is straightforward. In regions where algorithm confidence is less certain, however, (i.e. dense boreal forest) interpretation of the Tbs (particularly in a temporal sense) can assist in distinguishing the influence of snow cover on the microwave emission. An additional problem in using the SWE retrievals is that in operational usage, the Environment Canada algorithm suite calculates per pixel SWE as a weighted average based on land cover. This can be problematic for grid cells with two dominant land covers (i.e. 50% prairie; 50% boreal). Both the prairie and boreal retrievals will be uncertain due to the influence of sub-grid land cover heterogeneity on microwave emission. The final grid cell SWE is then a weighted average of two uncertain retrievals (50% × prairie SWE; 50% × boreal SWE). Because of this issue, Environment Canada is presently revisiting how they derive the final grid cell SWE for heterogeneous grid cells. The current analysis focuses on data obtained daily from the beginning of the SSM/I satellite record (1987), to 2006.

The ancillary datasets used to assess the nature of Tb regimes are ecoprovinces. Ecoprovinces are ecological management units based on terrestrial characteristics, and were developed as part of the National Ecological Framework of Environment Canada (Rowe & Sheard, 1981; Wiken, 1986; Wiken et al., 1996). Ecoprovinces are largely based on characterizing major assemblages of structural or surface forms and faunal realms, as well as vegetation, hydrology, soil, and macro-climates (Marshall et al., 1998). These ecological units are useful for describing the major driving factors of an ecosystem, and as such are useful for conservation planning and analysis. We use these classifications as the baseline ecological management units with which to compare our derived Tb regimes. For a review of the history of ecological regionalization in Canada, see Bailey (1985). In addition, background and key concepts for the Ecological Framework of Canada are available at http://www.ec.gc.ca/soer-ree/English/Framework/default.cfm.

3. Methods

The annual and inter-annual temporal patterns of SWE are determined by application of existing spatial and temporal analysis methods to a long-term, spatially-referenced dataset on Tb differences. For the current analysis, daily Tb differences are obtained for each 25 km by 25 km grid cell in the dataset. Analysis is carried out over 19 years, providing a time-series of 6935 days of Tbs per grid cell (total of 5325 grid cells). As SWE is a seasonal variable, these time-series form cyclic SWE accumulation/melt curves. Smoothing functions are fit to the observed data, and the temporal components of each time-series are used to generate temporal metrics by treating each grid cell within the study region as a separate cyclic time-series. Several temporal metrics are integrated into a hierarchical, multivariate classification algorithm. The results of the classification are used to delineate SWE regimes, providing a means for defining SWE management units for both ecological and anthropogenic processes.

3.1. SWE curve fitting procedure

In order to capture patterns in the SWE time-series, various smoothing methods to reduce data fluctuations are used in practice. These methods include the use of weekly (e.g. Derksen et al., 2000a,b; Derksen et al., 2002; Derksen et al., 2000a,b), monthly (e.g. Derksen et al., 2005), and yearly (e.g. Wulder et al., 2007) running means. In addition, spatial averaging of SWE values has been used to reduce variability, as well as to examine relationships between SWE and atmospheric circulation (Derksen et al., 2000a,b). Most existing methods rely on data-reduction to correct for problems induced by the atmosphere, temperature, and the snow pack itself, and may over generalize important annual or inter-annual fluctuations in the Tb time-series. In addition, these methods do not take into account the

inherent properties of passive microwave derived Tb data, such as systematic and non-systematic underestimation of SWE.

One method which has been used in research on remotely sensed vegetation indices uses splines in a recursive setting to fit a continuous model to Normalized Difference Vegetation Index (NDVI) data (Bradley et al, 2007; Hermance, Jacob et al., 2007; Hermance, 2007). By recursively fitting high order splines to the data, the effects of drop-outs and spurious fluctuations in the data are reduced, and the local variation in vegetation temporal cycles captured. Applying a similar approach to SWE data should reduce problems associated with the effects of snow pack inhomogeneities and erroneous fluctuations in the Tb satellite record.

Smoothing splines are an indirect smoothing method based on penalized least squares, and define a continuous function using a series of polynomials fitted over adjacent time intervals along the SWE time-series (Green & Silverman, 1994). The function is constrained such that both the first and second derivatives, as well as the function itself are continuous at the intersections of the temporal intervals. Thus, for a given time-series y, a smoothing spline is used to model the data as

$$y_i = f(t_i) + \epsilon_i, \tag{1}$$

where f is some unknown smooth function of t, and ϵ represents independent and identically distributed errors. The estimate of f, f' is chosen so that it minimizes

$$\sum_{i=1}^{n} (y_i - f(x_i))^2 + \lambda \int (f''(t))^2 dt. \tag{2}$$

The smoothing parameter λ must be specified, and is used to control the exchange between observed data fidelity and curve smoothness, and represents the rate of exchange between the residual error, or data fidelity,

$$\sum_{i=1}^{n} (y_i - f(x_i))^2, \tag{3}$$

and the roughness of the curve,

$$\int (f''(t))^2 dt. \tag{4}$$

In the current example, λ is selected using generalized cross-validation. This is a common method for selecting smoothing parameters, and is simply a modified form of the usual cross-validation (see Green & Silverman, 1994; Craven & Wahba, 1979).

Due to the large variability in inter-annual Tb temporal characteristics, fitting a harmonic average annual base model to the Tb data, as in Hermance et al. (2007) and Hermance (2007), proved problematic. As such, both the initial and secondary models in the recursive spline algorithm applied here are fit using smoothing splines. Given that Tb returns tend to underestimate the actual amount of SWE on the landscape in many areas (Derksen et al., 2005), we employ a weighted least squares approximation for the second iteration of the spline fitting procedure in order to preferentially fit the upper envelope of the data. As in Hermance et al. (2007), residuals between the initial spline model and the Tb differences are computed from

$$\Delta d = d_{obs}(i) - d_{pred}(i), \tag{5}$$

where $d_{obs}(i)$ is the Tb difference, and $d_{pred}(i)$ is the value predicted by the initial spline model. A Gaussian-type weight is applied to each observed value based on

$$weight := \begin{cases} 0, & |\Delta(d)_i| \geq 15 \\ \exp\left(-sign\left(\frac{|\Delta d|}{w}\right)^2\right), & |\Delta(d)_i| < 15 \end{cases}, \tag{6}$$

where w is a parameter used to control the width of the Gaussian operator, and for the current application is set at 5 Tbs, sign is an operator whose value is -1 for negative Δd and $+1$ for positive Δd, and the effects of spurious outlying Tb differences (greater than 15 K from initial fitted curve) due to confounding snow properties such as wet snow, were controlled by setting their weights equal to zero. The computed weights are applied to each observed value in the dataset for the second iteration of the spline algorithm, producing a smoothed, continuous, penalized weighted least squares approximation of the Tb temporal signature for each grid cell in the dataset.

3.2. Derivation of seasonal temporal metrics

A discrete moving window, with a width based on the observed periodic nature of the Tb time-series (365 days), is used to compute the suite of temporal metrics for each SWE season. The temporal components that are computed from the time-series are given in Table 1, and are adapted from Lloyd (1990), Malingreau (1986), and Reed et al. (1994). For each grid cell, temporal trends are summarized using 12 different temporal metrics, summarized annually (12 metrics × 19 years), and are represented graphically in Fig. 2 and will be described below. By computing each metric for each year in the study period, we are able to investigate inter-annual variability in the computed metrics.

Derivation of the temporal metrics is based on the properties of the smoothed curve used to represent the Tb differences through time. To derive the start of the SWE accumulation season (SACC), we use the first negative turning point (trough) of the second derivative of the smoothed Tb difference curve within each discrete temporal window (Fig. 3C). Similarly, to compute the start (SMEL) and end (EMEL) of the SWE melt season, we use the global (within the moving window) maximum and minimum second derivative of the smoothed Tb difference curve within each discrete temporal window respectively (Fig. 3C). The start and end of melt season for the current analysis represents the start and end of the major melt events, as opposed to early-season melt due to fluctuating temperatures, or freeze–thaw interactions.

The time integrated SWE (TINS), or seasonal sum of Tb values, is the area under the smoothed Tb difference curve between the start of the accumulation season and the end of the melt period (Fig. 3A). In addition, the values of the first derivative of the smoothed spline curve are used to compute both accumulation (RACC) and melt

Table 1
Each of the 12 temporal metrics are computed for each grid cell in the study region, for all 19 years of the study period.

| Metric	Description	Derivation
SACC	Start of SWE accumulation season	First negative turning point (trough) of the second derivative of the smoothed curve
EMEL	End of SWE melt season	Global (within moving window) minimum of the second derivative of the smoothed curve
SMEL	Start of SWE melt season	Global (within moving window) maximum of the second derivative of the smoothed curve
TINS	Time integrated SWE (Sum of SWE)	Area under the smoothed SWE curve between the SACC and EMEL
RACC	Rate of SWE accumulation	Mean value of the first derivative during accumulation season
RMEL	Rate of SWE melt	Mean value of the first derivative during melt season
SLEN	Length of SWE season	Time between SACC and EMEL
TMAX	Timing of maximum SWE	Time of maximum value of the smoothed curve between SACC and EMEL
TMIN	Timing of minimum SWE	Time of minimum value of the smoothed curve between SACC and EMEL
MAXS	Maximum SWE value	Maximum value of the smoothed curve between SACC and EMEL
MINS	Minimum SWE value	Minimum value of the smoothed curve between SACC and EMEL
RNGS	Range of SWE values	Range between MINS and MAXS
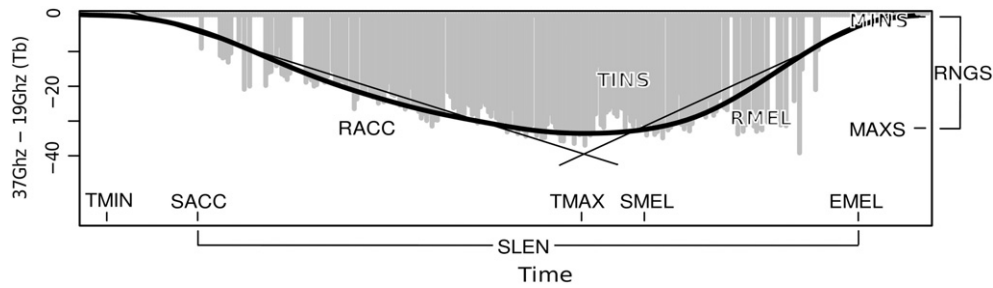
Fig. 2. Graphical representation of the 12 computed temporal metrics. Acronym definitions given in Table 1.

(RMEL) rates (Fig. 3B). For the current analysis, rates are defined as the mean value of the first derivative during each subsequent season. In other words, the accumulation rate is the average slope of the smoothed spline curve during the accumulation season, and the melt rate is similarly defined for the melt season.

The remaining 6 temporal metrics are derived directly from the smoothed Tb difference curve, and are based on the previously computed metrics (Fig. 3A). The length of the SWE season (SLEN) is calculated as the time from the start of the accumulation season to the end of the melt period. Season length is then used to constrain the values and dates of the maximum (TMAX, MAXS) and minimum (TMIN, MINS) Tb differences. Building on these metrics, the Tb difference range is the range between minimum and maximum Tb differences (MAXS–MINS) in a given year (RNGS).

It is important to note that the metrics presented here may not necessarily correspond directly with the true SWE conditions on the ground surface, but rather, are a representation of the SWE temporal dynamics (Bradley et al., 2007). The exact date, value, and characteristic that an individual temporal metric relates to may not be precise given the spatial resolution provided by this dataset; however, it provides an indication of the spatial–temporal dynamics, and differences in the temporal dynamics of SWE.

3.3. Analysis of temporal metrics

In order to reduce data redundancy caused by correlated temporal metrics and aid interpretability of results, we limit the number of temporal metrics used in the final hierarchical cluster analysis based on ecological significance and data characteristics. Ecological significance of the three metrics retained will be discussed below. The metrics used include: (a) the coefficient of variation in melt rates (CMR), providing a perspective on temporal changes in SWE due to
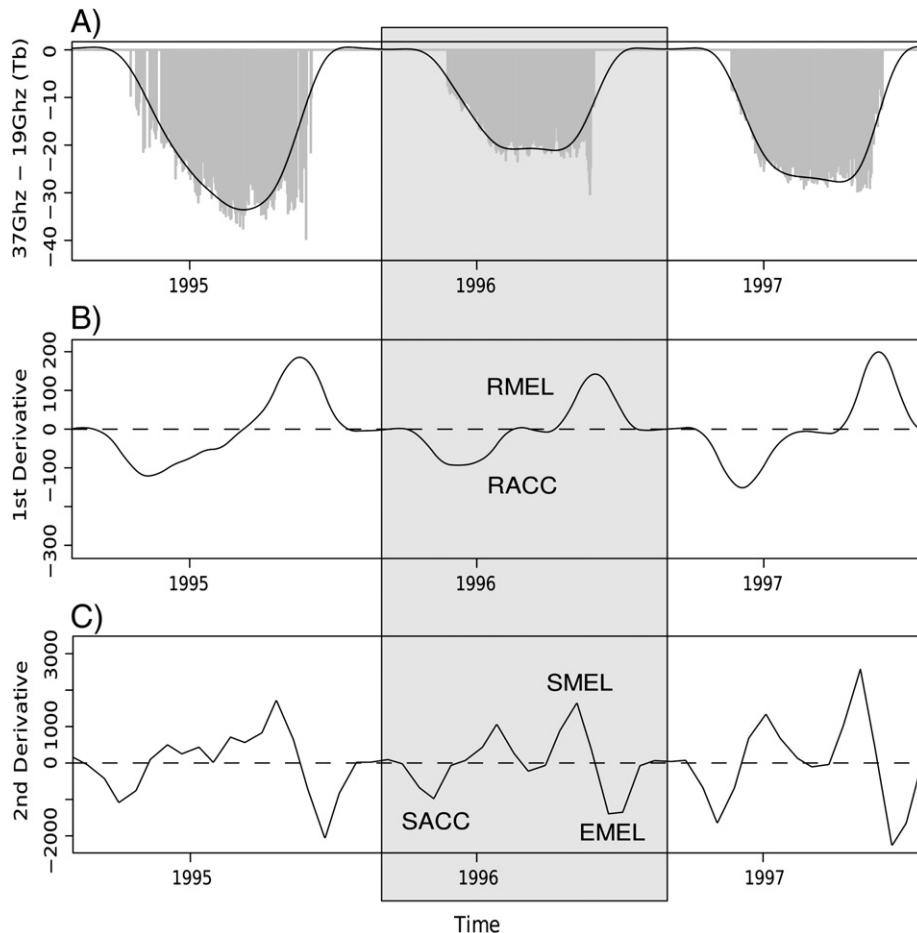

Fig. 3. Hypothetical representation of the 12 temporal metrics. Metrics are based in the properties of the smoothed curve used to represent the SWE values through time, including the values of the curve itself, as well as the 1st and 2nd derivatives. Grey shaded area represents one discrete temporal window.

climate; (b) the annual maximum Tb difference (AMS), indicating the water storage levels along the time-series; and (c) the coefficient of variation in time integrated SWE (CTS), which is the sum of all measured Tb differences, and represents the variability in snow pack development over the time-series. Using the full 19 year time-series, we compute the mean (AMS), and CV (CMR and CTS) for the three temporal metrics and ensured that these metrics were uncorrelated as determined using a standard correlation matrix.

Snow melt rates, represented by CMR, strongly influence the timing and length of the SWE season, both acting to control seasonal vegetation growing patterns (e.g. Walker et al., 1999; Kudo, 1991; Walther et al., 2002; McCarty, 2001) and animal habitats (e.g. Karl et al., 1993). From a climate change perspective, significant changes in the rates of snow melt may cause a shift in the overall snow cover season, a change in the total duration of the snow season, or a change in overall snow seasonality. Characterizing variability of melt rates is therefore important for identifying the response of snow cover and SWE to climate change. This makes CMR a useful variable to consider when distinguishing regional variations in SWE temporal character-istics, as regional variations in CMR will highlight areas differentially impacted by changes in temperature and humidity induce by changing climate conditions.

While the variability of melt events is important for characterizing changes induced by climate, it does not address water storage, which is important for flood forecasting, water resource management, and hydroelectric power generation (Pulliainen & Halliskainen, 2001; Chang et al., 2003). Water storage is represented by the AMS metric, and is an important indicator of spring runoff which controls surface water availability for a region. Regardless of the rate and amount of snow accumulation and precipitation over a region, variations in the capacity of an area to store water will have major consequences for the surrounding regions, and will ultimately highlight major differences in SWE regimes. Conversely, the CTS metric provides an indication of the variability in characteristics of snow pack develop-ment and a means to estimate SWE seasonal activity. While it may be difficult to directly determine whether a region experienced steady or varied snowfall events, or whether there are changes over time in the nature of snowfall events (i.e. an increase in extreme snowfall events or trace precipitation events), these characteristics will be indirectly reflected in CTS.

3.4. Hierarchical cluster analysis

Hierarchical cluster analysis has been used for a range of applications, including ecological analyses (McKenna, 2003; Nemec & Brinkhurst, 1988), hydrological regionalization (Rao & Srinivas, 2006; Poff, 1996), and climate zone delineation (Gong & Richman, 1995; Unal et al., 2003). Cluster analysis in its most general form is a method for identifying patterns within multivariate data (Sneath & Sokal, 1973; Kaufman & Rousseeuw, 1990), and more specifically, it involves recursively grouping similar objects based on multivariate attributes into groups. There are a range of methods for assessing similarity of objects or groups with cluster analysis, and different approaches will highlight different aspects of a dataset (McKenna, 2003; Johnston, 1976). Measures of similarity based on Euclidean distances in attribute space are common in the ecological literature (e.g. Fovell & Fovell, 1993; Gong & Richman, 1995; Nemec & Brinkhurst, 1988), and as such, we compute similarity of grid cells based on Euclidean distance in the three temporal metrics (CMR, AMS, and CTS). In addition to the measure of (dis)similarity, hierarchical cluster analysis requires linkages between previously formed clusters (aspatial) to be measured and assessed for merging. This in effect dictates how higher-level fusions are executed (McKenna, 2003). For the current analysis, we use an average linkage agglomerative clustering algorithm, which computes the distance between two clusters as the average measured distance between all pairs of objects,

in this case grid cells, between the two clusters. For our dataset, consisting of $n = 3$ temporal metrics, we generate a similarity matrix $\boldsymbol{D}$ using,

$$d_{ij} = \sqrt{\sum_{k=1}^{n}(x_{ik} - x_{jk})^2},$$

(7)

where d_{ij} is the Euclidean distance in attribute space between the normalized values of grid cell i and j, $j \neq i$. From this, linkages between clusters are assessed based on

$$d_{lm} = \frac{1}{N_l N_m}\sum\sum d_{ij},$$

(8)

where d_{ij} is the Euclidean distance in attribute space between grid cell i in cluster l and grid cell j in cluster m, and N_l and N_m are the number of grid cells in clusters l and m respectively. The cluster grouping that minimizes d_{lm} is then used to group the clusters. This process is performed recursively until a single cluster remains, providing a hierarchical grouping of grid cells based on their associated temporal metrics. As the clusters are grouped to form increasingly larger clusters, a hierarchical grouping tree known as a dendrogram is generated, providing a visual representation of the hierarchy of Tb difference clusters at various scales. Each node in the dendrogram occurs at a specified height, which is defined as the linkage distance between the two children clusters. The dendrogram is used to assess the relevance of the clusters, allowing us to reject clusters which contain few grid cells or clusters of grid cells that are spatially dispersed.

Once the dendrogram has been formed, we must distinguish be-tween clusters that reflect relationships of the phenomena repre-sented by the data, and those generated as a result of random effects and/or data uncertainties (Nemec & Brinkhurst, 1988; McKenna, 2003). There are several methods that use the statistical properties of the data to assess significance of clusters (Smith & Dubes, 1980; McKenna, 2003; Milligan & Cooper, 1985; Pillar, 1999). One such method employs bootstrap resampling to assess the stability of detected clusters (Hennig, 2007; McKenna, 2003; Efron et al., 1996; Felsenstein, 1985). This type of analysis is beneficial because it explicitly considers the variability within our input dataset, and does not rely on any predefined distribution to assess cluster significance. Bootstrap resampling (Efron, 1979) applied to hierarchical cluster analysis has been used in a number of analyses attempting to assess the appropriateness of a particular hierarchical arrangement (Hennig, 2007; Ellis et al., 1991; Pillar, 1999; McKenna, 2001; Kerr & Churchill, 2001). In its most basic form, bootstrap resampling for hierarchical cluster analysis involves generating a number of random 'bootstrap samples' from the original dataset, and creating bootstrap replicates of the dendrogram by applying the hierarchical cluster analysis to the bootstrap samples. These dendrogram replicates are each compared with the initial hierarchical assemblage, and significance is based on the proportion of dendrogram replicates that are similar to the initial dendrogram. For a comprehensive review of methods for bootstrap hierarchical cluster analysis, see Efron et al. (1996) and Nemec and Brinkhurst (1988).

Bootstrap resampling has been refined to enable the stability of the hierarchical classification to be determined by considering the stability of each individual cluster (Hennig, 2007). For example, a number of bootstrap replicates of the initial dendrogram are created as above, and for each cluster in the initial dendrogram, the most similar cluster in each bootstrap replicate is found using the Jaccard coefficient (Jaccard, 1901) as a measure of similarity. The Jaccard coefficient is defined as the size of the intersection divided by the size of the union of the sample sets, and is used here to measure the similarity between cluster hierarchies. The level of similarity is recorded, and stability for each cluster is assessed based on the mean similarity over all resampled datasets. This is done to ensure

that only meaningful clusters are identified, leaving spurious clusters to be assessed individually by the analyst. In the current example, these clusters can be combined with the geographically nearest valid clusters to maintain spatial contiguity of observed clusters, reducing the effects of spurious clusters on the final SWE regime delineation. An additional benefit is that relative to other bootstrap approaches, determining the 'optimal' number of clusters via this method requires fewer bootstrap replications to produce valid results (Hennig, 2007). As such, we use Hennig's cluster-wise assessment of stability to determine the 'optimal' number, and configuration of SWE regimes across the Canadian Prairies. By constraining the number of possible clusters to be close to the number of current ecoprovinces (between 15 and 25), we select the final hierarchical dendrogram based on the cluster arrangement that maximizes the proportion of stable clusters, using a mean Jaccard coefficient cutoff of 0.5 (Hennig, 2007). As suggested by Everitt (1974), metric values were normalized prior to integration via hierarchical cluster analysis.

3.5. Comparison with ecoprovinces

In order to assess the differences between the hierarchically defined SWE regimes and current summer based ecological management units (based on terrestrial ecoprovinces), we examine the spatial correspondence between these two landscape partitioning methods. Comparing units defined using winter and summer conditions will provide an indication of how well winter processes are represented by traditional ecological management units and may provide insights for improving winter-based modeling and research efforts. At the current scale of analysis, ecoprovinces represent the most appropriate comparison with SWE regimes, as they are designed to capture major structural assemblages and macro-climates (Marshall et al., 1998), which both tend to have a strong influence on snow deposition and accumulation.

The comparison of SWE regimes with ecoprovinces is done by intersecting the boundaries of both regions, and considering the distribution of values within each ecoprovince on a pixel-by-pixel basis. We then highlight ecoprovinces with relatively high and/or relatively low numbers of different SWE regimes within its boundaries.

4. Results

4.1. Temporal metrics

The spatial and frequency distributions for the three temporal metrics (CMR, AMS, and CTS) are given in Fig. 4a, b, and c, along with a combined composite image of the three metrics in Fig. 5. The composite image reflects the combined conditions of the three temporal metrics by assigning each metric to a different colour band, Similar to Coops et al. (2008), in which they examine where annual cumulative greenness, minimal annual vegetation cover, and vegetation seasonality are correlated, and where they differ, this provides a visualization of the three temporal metrics, highlighting how the components combine to form the overall spatial patterns of SWE Tb differences across the landscape. Over the study region, melt rates range from approximately −17.18 K/day to −8.01 K/day (equivalent to 23.80–0.04 cm/day), with the majority of the study region experiencing melt rates of approximately −11.97 K/day (10.32 cm/day). As a result, CMR (coefficient of variation) values range from approximately 0.07 to 1.02. Regional variations in the variability of CMR highlight a large area towards the south-central portion of the study region where melt rates are highly variable relative to the mean melt rate for the entire study region (Fig. 4A). On the western side of this region, there is an abrupt change to more stable CMR conditions, whereas the portion of the study area to the east of this highly variable region experiences smoother transitions to more stable conditions. Conversely, the northern portion
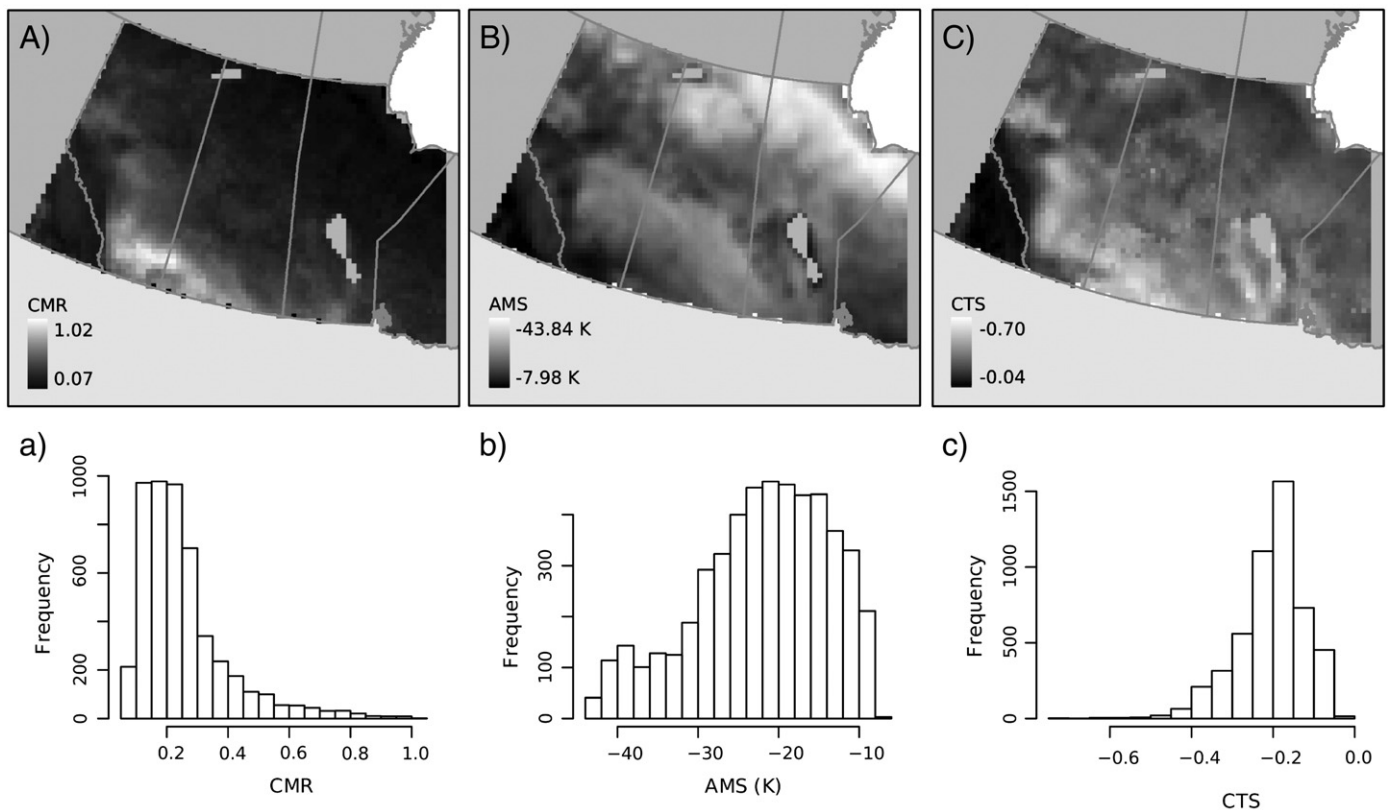
Fig. 4. The spatial and frequency distribution of values for the three temporal metrics; Variability in SWE melt rates (A, a), providing a perspective on temporal changes in SWE due to climate, annual mean maximum SWE (B, b), indicating the water storage levels along the time-series, and variability in SWE seasonal activity (C, c), which is the sum of all measured Tb differences, and represents the variability in snow pack development over the time-series.
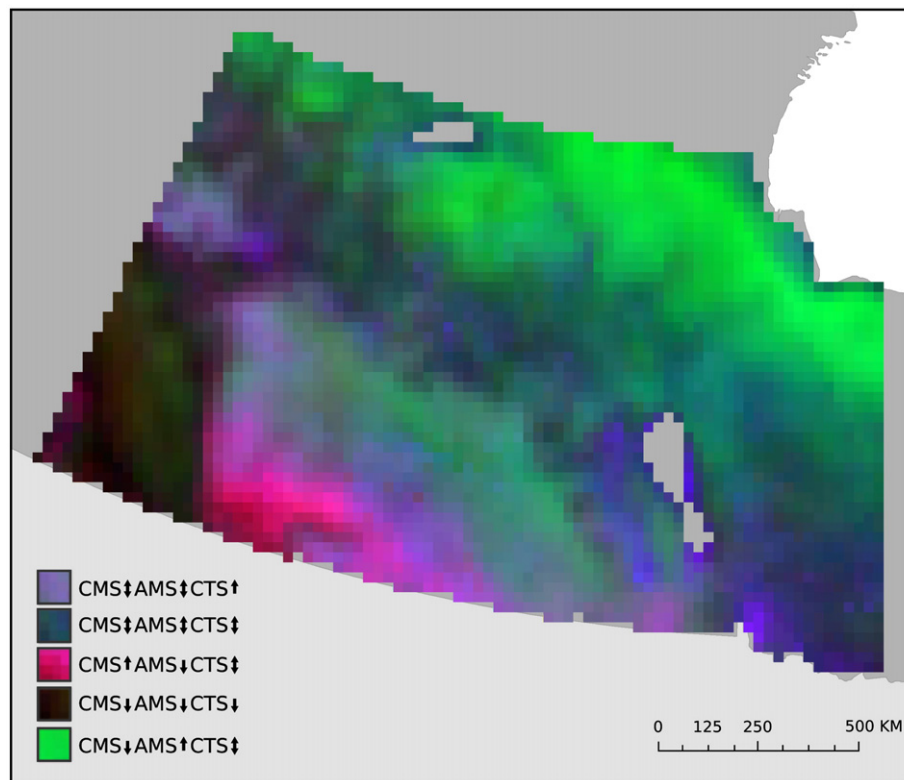
Fig. 5. Composite image of the combined temporal metrics; derived from assigning CMR to the red band, AMS to the green band, and CTS to the blue band. Ecoprovince boundaries are overlain in grey, highlighting the variability in correspondence between the spatial patterns presented by the metrics, and the spatial distribution of ecoprovinces. Note: ↑ indicates high, ↓ indicates low, and ↕ indicates moderate values of each corresponding metric. For all three colour bands, darker values represent higher levels of the corresponding temporal metric. For example: light green represents areas of stable, relatively wet snow conditions, with active seasonal changes, dark purple denotes average values for all three metrics, and dark browns and greens represent highly variable melt rates, low annual Tb differences, and low seasonal activity. (For interpretation of the references to colour in this figure legend, the reader is referred to the web version of this article.)

of the study area is largely characterized by relatively stable CMR throughout the measured time-series.

For AMS, differences in Tbs range from −43.84 K to −7.98 K corresponding to approximately 92.85 mm to 0.00 mm in the open Prairies. Values are normally distributed, with a mean of −22.04 K. Regions of low AMS generally occur in the south-west portion of the study region (Fig. 4B), and there is a general trend of increasing AMS towards the north-east. Two bands of relatively high AMS occur over the central and northern reaches of the study region, both with a north-east to north-west orientation. These bands correspond with regions of relatively high annual precipitation, and long, cold winters with continuous snow cover. Conversely, regional trends are less pronounced with CTS than with AMS, with smaller patches of high variability occurring throughout the central portion of the study region (Fig. 4C). The frequency distribution of values for CTS is slightly skewed (skewness = 0.88), and values range from −0.04 to −0.70 (Fig. 4c). In general, large CTS values occur over regions of high AMS. However, these large values also appear to be relatively stable, occurring to a large degree over the stable band of CTS in the north-east portion of the study region, west of Hudsons Bay. Regions of high values occur at the base of the Rocky Mountains, in some cases extending towards central Alberta and across the international boarder to the south.

In Fig. 5, variability in melt rates (CMR) is assigned to the red band, whereas water storage, or annual maximum SWE (AMS) is assigned to the green band, and SWE seasonal activity, represented by the coefficient of variation in time integrated Tb differences (CTS), is assigned to the blue band. In all three cases, darker values represent higher levels of the temporal metric. As such, the large regions of light green to the north of the study region represent areas of stable, relatively wet snow conditions, with active seasonal changes, whereas regions displaying average values for all three metrics are shown in

dark purple. In contrast, the regions of highly variable melt rates, low annual Tb differences, and low seasonal activity to the west combine to produce dark browns and greens. The elongated band of light greens and blue towards the center of the study region is composed primarily of relatively stable melt rates, average amounts of SWE available for melt, and highly active seasonal variations, contrasting with the dry, extremely variable conditions to the south, and wet, stable regional patterns to the north.

4.2. Hierarchical cluster analysis

The hierarchical cluster arrangement with the highest proportion of stable clusters delineates 18 clusters which form the basis of our SWE regimes. This arrangement occurs at a clustering height of approximately 1.3 with cluster sizes ranging from 823 to 4 grid cells. All 18 clusters are listed in Table 2, with summary statistics computed over all grid cells located within each cluster for each of the three temporal metrics.

The first two clusters in the hierarchical arrangement are characterized by average levels of variability in terms of melt rates, and relatively low mean maximum Tb difference. The variability in seasonal Tb difference activity in these regions is relatively close to the study area mean, though the distribution of values is highly skewed towards less stable conditions. These traits are particularly pronounced in the first cluster, which occupies the lower south-eastern slopes of the Rocky Mountains and the western edge of the Alberta Plains, and to a lesser degree, some extremely dry highland regions of the Rocky Mountains.

Clusters located over the open grasslands in the Interior Plains of Canada exhibit a distinctive pattern whereby a slow gradient in the values of three temporal metrics is exhibited (as we move from clusters

Table 2
Summary of temporal metrics for each hierarchical cluster.

Cluster	Metric	Mean	Median	StdDev	Min	Max	Cluster	Metric	Mean	Median	StdDev	Min	Max
1	CMR	0.22	0.22	0.04	0.12	0.33	10	CMR	0.61	0.60	0.05	0.54	0.70
	AMS	−11.29	−11.62	2.10	−15.97	−6.75		AMS	−14.71	−14.25	1.42	−17.77	−13.27
	CTS	−0.08	−0.07	0.03	−0.18	−0.04		CTS	−0.29	−0.29	0.02	−0.31	−0.25
2	CMR	0.39	0.39	0.02	0.34	0.46	11	CMR	0.70	0.69	0.07	0.56	0.86
	AMS	−12.35	−12.87	2.89	−16.26	−7.14		AMS	−16.69	−16.55	1.78	−21.11	−12.50
	CTS	−0.18	−0.19	0.04	−0.25	−0.11		CTS	−0.39	−0.39	0.03	−0.48	−0.32
3	CMR	0.25	0.24	0.04	0.15	0.37	12	CMR	0.94	0.94	0.04	0.86	1.02
	AMS	−17.04	−17.20	2.59	−23.46	−10.47		AMS	−12.33	−12.06	1.25	−14.68	−10.32
	CTS	−0.20	−0.20	0.03	−0.26	−0.13		CTS	−0.34	−0.35	0.04	−0.40	−0.28
4	CMR	0.25	0.25	NA	0.25	0.25	13	CMR	0.14	0.13	0.03	0.08	0.24
	AMS	−16.57	−16.57	NA	−16.57	−16.57		AMS	−32.05	−32.02	3.03	−38.36	−25.50
	CTS	−0.07	−0.07	NA	−0.07	−0.07		CTS	−0.18	−0.18	0.03	−0.26	−0.11
5	CMR	0.40	0.40	0.04	0.31	0.54	14	CMR	0.29	0.29	0.03	0.22	0.41
	AMS	−22.20	−22.70	2.58	−26.98	−13.90		AMS	−14.92	−15.25	1.85	−19.27	−9.91
	CTS	−0.28	−0.29	0.03	−0.34	−0.21		CTS	−0.28	−0.27	0.03	−0.34	−0.24
6	CMR	0.47	0.48	0.07	0.29	0.59	15	CMR	0.28	0.28	0.04	0.17	0.37
	AMS	−20.25	−20.63	2.70	−24.80	−11.08		AMS	−25.07	−25.67	2.79	−29.75	−17.34
	CTS	−0.35	−0.35	0.02	−0.42	−0.31		CTS	−0.26	−0.26	0.02	−0.33	−0.20
7	CMR	0.16	0.15	0.03	0.09	0.26	16	CMR	0.10	0.10	0.01	0.07	0.13
	AMS	−23.31	−23.33	2.03	−28.87	−18.46		AMS	−40.04	−39.85	1.54	−43.84	−37.11
	CTS	−0.20	−0.20	0.03	−0.27	−0.14		CTS	−0.16	−0.16	0.02	−0.22	−0.11
8	CMR	0.61	0.59	0.07	0.49	0.77	17	CMR	0.41	0.42	0.03	0.37	0.45
	AMS	−10.15	−9.84	1.39	−13.01	−7.99		AMS	−15.16	−15.96	2.92	−19.43	−11.65
	CTS	−0.18	−0.17	0.03	−0.24	−0.14		CTS	−0.43	−0.43	0.02	−0.48	−0.40
9	CMR	0.82	0.83	0.05	0.72	0.91	18	CMR	0.52	0.52	0.02	0.50	0.55
	AMS	−10.34	−10.17	1.26	−13.12	−8.63		AMS	−11.48	−11.46	0.58	−12.12	−10.88
	CTS	−0.24	−0.24	0.02	−0.30	−0.21		CTS	−0.50	−0.49	0.02	−0.53	−0.49

8 and 9, through 12, 11, 6, and 5 to 15). Clusters 8, 9, and 12 are characterized by some of the highest variability in melt rates across the study area, as well as average variability in seasonal activity, and consistently low maximum Tb differences. Conversely, clusters 11 and 6 appear to be part of a transition zone between the high variability in melt rates to the south, and more stable conditions to the north. This is reflected in the decrease in variability of melt rates, and maximum Tb differences towards clusters 5 and 15, where melt rates are once again close to the mean for the entire study region, and maximum Tb difference tends to be significantly lower than surrounding regions. Variability in Tb difference seasonal activity throughout these two regions is consistently low, indicating that SWE processes are more stable here.

North of this prairie region is cluster 3, which has the largest cluster area, and includes much of central Canada. Values for all three temporal metrics in cluster 3 are close to the mean for the entire study region. Cluster 3 occupies approximately 22.80% of the overall study region, stretching from south-western Manitoba, through to northern Alberta, with an additional branch extending into central Alberta, along the base of the Rocky Mountains. North-west of this central region are three clusters which show strong linear spatial patterns stretching from northern Ontario to northern Saskatchewan, and in some cases as far as northern Alberta. This region is composed of clusters 7, 13, and 16, and is typified by significantly low variability in melt rates, extreme high maximum SWE values, and relatively high levels of variability in Tb difference seasonal activity. These characteristics are particularly significant in cluster 16, which lies at the northern extreme of the study region.

The remaining 5 clusters (4, 10, 14, 17, 18) each occupy no more than 4.35% of the total study region, for a total coverage of approximately 5.21%. These clusters occur over regions of rapidly changing gradients for all three metrics, and appear to highlight unique SWE regimes. Cluster 14 appears to be unique from all other remaining clusters, though it is characterized by conditions similar to some regions located over the southern Prairies, such as increased variability in both melt rates and seasonal activity, with significantly low maximum Tb differences. Spatially, it occurs as 5 separate regions, located along the same linear band as cluster 3. These regions include

two larger domains which occur over south-eastern Ontario, one region west of Lake Winnipeg, and two smaller regions in central Saskatoon and northern Alberta respectively. Cluster 14, along with clusters 11 through 18, form a unique grouping of grid cells based on their configuration of the three temporal metrics, and were not joined with the remaining clusters until a grouping height of 3.06 in the hierarchical cluster analysis.

4.3. Comparison with ecoprovinces

A pixel-based summary of the variation in SWE regimes by ecoprovince (Fig. 6) yields the results in Table 3. Upon examining the spatial correspondence between summer and winter partitioning methods, it is clear that there is variability in how well winter processes are represented by the various ecoprovinces. The number of different SWE regimes located within a single ecoprovince ranges from 2 in the Hudson-James Lowlands (15.2) and Southern Montane Cordillera (14.3), to 10 in the Eastern Boreal Plains (9.3), though the ecoprovinces with very few clusters tended to be located towards the edges of the study region. The largest correspondence in terms of percentage coverage of a single cluster is located over the Northern Montane Cordillera (14.4) ecoprovince, where 92.02% of the ecoregion is captured by cluster 1. Similarly high levels of correspondence occur in the northern portion of the study area, where the Western Boreal Shield (6.1) ecoprovince is covered to a large degree by clusters 7 (45.86%) and 13 (39.94%), and the Western Taiga Shield (5.1) and Western Boreal Shield (15.2) ecoprovinces are able to capture 92.86% of cluster 16, and large portions of cluster 13.

Regions where ecoprovinces have more variability in associated SWE regimes occur towards the central and southern portions of the study region. Despite the large size and widespread linear spatial patterns of clusters 6, 5, 15, and 3 throughout this central region, the ecoprovinces are unable to capture the major patterns in Tb differences that they represent. For example, both the largest and smallest of these clusters (3 and 6) are spread across 9 different ecoprovinces each. In addition, the Parkland Prairies (10.2) and Central Grasslands (10.3) ecoprovinces of the Prairies ecozone appear to miss major Tb difference spatial–temporal patterns, containing portions of
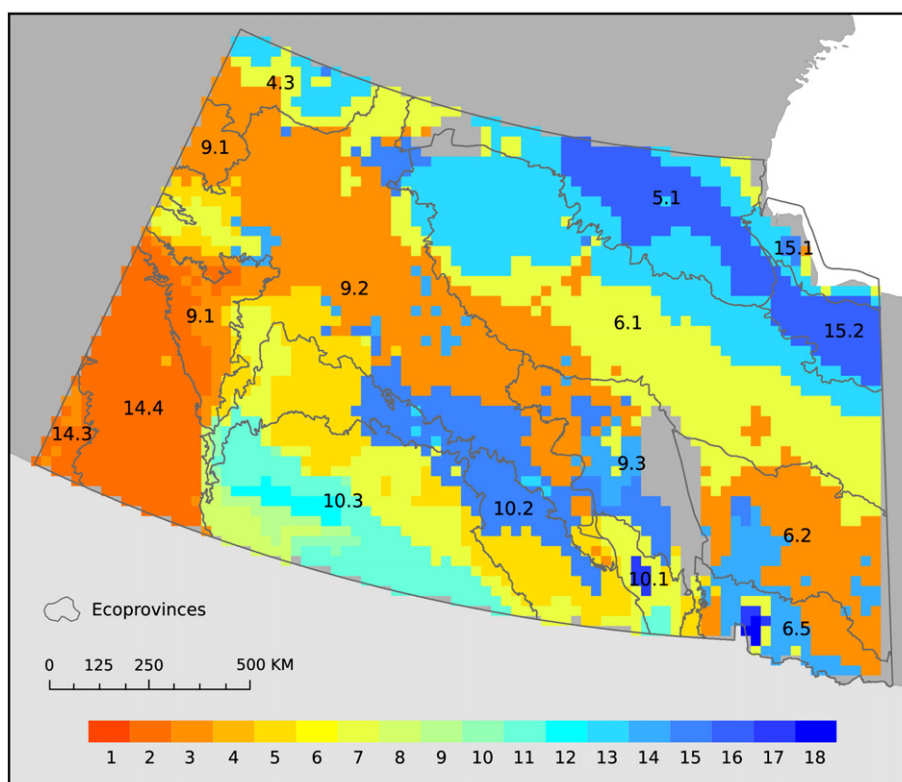
Fig. 6. Examining the spatial correspondence between hierarchical clusters and ecoprovinces: 4.3: Hay-Slave Lowlands; 9.1: Boreal Foothills; 9.2: Central Boreal Plains; 9.3: Eastern Boreal Plains; 14.4: Columbia Montane Cordillera; 14.3: Southern Montane Cordillera; 10.3: Central Grassland; 10.2: Parkland Prairies; 10.1: Eastern Prairies; 6.1: Western Boreal Shield; 6.2: Mid-Boreal Shield; 6.5: Eastern Boreal Plains; 5.1: Western Taiga Shield; 15.1: Hudson Bay Coastal Plains; 15.2: Hudson-James Lowlands.

5 and 9 different clusters respectively. Several of the smaller eco-provinces towards the south-western edge of the study region (10.1, 9.3, 6.2, and 6.5) contain a large number of different clusters as well, though this is due in part to the larger variability in the spatial arrangement of clusters in this region.

5. Discussion

There is a strong spatial component to the geographic distribution of the three temporal metrics presented in this analysis, and spatial patterns are captured in the delineation of SWE regimes via hierarchical multivariate clustering. The spatial distribution of the three temporal metrics appeared to capture SWE spatial–temporal

processes which, to a large degree, are unaccounted for in terrestrial ecoprovinces. The spatial disconnect between ecoprovinces, and homogeneity in spatial–temporal SWE patterns is evidence that winter-based processes are not sufficiently represented by current ecological management units in Canada.

The hierarchical cluster analysis successfully incorporated different aspects of T_b difference temporal characteristics to yield distinct geographical regions useful for understanding the winter-based processes. Emphasis was placed on the temporal relationships within individual regions in order to highlight their unique spatial–temporal attributes. Despite this emphasis, there remain some large-area spatial trends in the temporal metrics, as well as in the overall SWE spatial temporal patterns that occur across the entire study region. As

Table 3
Thematic summary of the hierarchical cluster analysis results by ecoprovince; values represent the percentage composition of each of the ecoprovinces in terms of the 18 clusters.

Ecoprovince	Clusters																	
	1	2	3	4	5	6	7	8	9	10	11	12	13	14	15	16	17	18
4.3	0	0	31.31	0	0	0	33.33	0	0	0	0	0	33.33	0	1.01	0	0	0
5.1	0	0	1.09	0	0	0	9.06	0	0	0	0	0	40.22	0	0.72	48.19	0	0
6.1	0	0	11.69	0	0	0	45.86	0	0	0	0	0	39.94	0.15	1.18	0.74	0	0
6.2	0	0	59.4	0	0	0	18.05	0	0	0	0	0	0	18.8	2.26	0	0	0
6.5	0.84	0	37.82	0	3.36	6.72	0	0	0	0	0	0	0	42.86	0	0	2.52	1.68
9.1	31.76	12.16	37.16	0	6.76	5.41	0	2.03	0	0	0	0	0	0.68	0	0	0	0
9.2	0.28	0.84	52.88	0	12.52	6.33	6.33	0	0	0.14	0	0	1.55	3.94	14.21	0	0	0
9.3	0	0	30.38	0	4.43	10.13	8.23	0	0	0	0	0	0	16.46	25.32	0	0	0
10.1	0	0	0	0	14.52	46.77	0	0	0	0	14.52	0	0	0	0	0	9.68	0
10.2	0	0	0	0	44.91	11.93	0.35	0	0	1.05	1.75	0	1.4	0	34.04	0	0	0
10.3	0	0	0	0	14.95	23.53	0.25	8.58	5.15	2.94	32.84	4.9	0	0	4.17	0	0	0
14.3	39.47	28.95	0	0	0	0	0	0	0	0	0	0	0	0	0	0	0	0
14.4	92.02	0.84	0	0.42	0	0	0	1.26	0	0	0	0	0	0	0	0	0	0
15.1	0	0	1.92	0	0	0	5.77	0	0	0	0	0	42.31	0	9.62	13.46	0	0
15.2	0	0	0	0	0	0	0	0	0	0	0	0	10	0	0	75	0	0

Note: percentages do not necessarily add to 100% due to lakes, and other water bodies.

a result, similarities in the spatial patterns of SWE regimes were observed, highlighting strong north-west to south-east linear patterns across much of the study region, similar to the accumulation zone described in Derksen et al. (2000b). In addition to this, the Rocky Mountains along the western boarder of the study region have a clear influence on the spatial patterning of SWE across large portions of the prairies. These regional patterns are similar in extent and orientation to portions of the Alpine, Prairie, Taiga, and Tundra regions of Sturm et al. (1995), and may be highlighting some of the same spatially varying relationships that the Sturm et al. (1995) classification system was based upon (temperature, wind, and precipitation).

As is evidenced by the current analysis, while the terrestrial eco-provinces are able to characterize some of the variability and trends in the temporal characteristics of SWE, to a large degree these ecological units do not provide sufficient explanation for the observed temporal patterns on their own. In other words, the SWE spatial–temporal patterns generated as a result of this analysis have the potential to add a level of explanation to current ecoprovince boundaries. This is especially prevalent in the central and southern prairie regions, where high variability in melt rates and seasonal activity, combined with an abundance of SWE, provide highly sensitive regions with strong Tb difference gradients. This indicates that where SWE is most abundant and variable, current ecological units will be problematic for use when investigating winter-based processes. This is corroborated by the comparison between SWE regimes and ecoprovinces, which indicates that clusters with both high and low maximum Tb differences over regions of relatively low variability in melt rates and seasonal activity had a higher correspondence than similar regions with relatively high variability.

In some areas, ecoprovinces are appropriate for assessing winter-based processes. Where Tb differences tend to be low and variability minimal, regions based on spring and summer conditions provide an acceptable representation of winter processes. Examples of this include ecoprovinces along the western extent of the study area, and north of the prairies towards the Boreal Plains and Boreal Shield. In these ecoprovinces correspondence with SWE regimes was high, and ranged between 48.19% and 92.02%. This finding is in line with those suggested by Wulder et al. (2007), where they discuss a north-west to south-east zone of relatively stable SWE conditions across the boreal forest which tended to be resistant to climate variability through time. According to Derksen et al. (1998c) this zone appears to correspond with the direction of atmospheric airflow based on the 500 mb geopotential height field.

The SWE regimes generated as a result of this type of analysis should be used as guidelines for developing winter-based management units in conjunction with current ecological classifications. Regions where correspondence is weak, such as in the prairies and southern boreal plains, may warrant reconsideration, or require tailoring for specific modeling or management applications. Conversely, regions of high correspondence, such as those located west of central Alberta and towards the Hudsons Bay, may be sufficient for examining winter-based processes in their current state.

6. Conclusion

The methods presented in this research provide tools for spatially explicit analysis of long time-series datasets derived from satellite imagery. We utilize methods from time-series analysis, geographic information systems (GIS), ecosystem classification, and remote sensing to provide a unified perspective on the spatial–temporal interactions of SWE. Results are useful for environmental monitoring of SWE and SWE processes, as well as winter-based modeling and research. In addition, the results from this research present opportunities for modeling spatial processes that are year long. For instance, summer processes can be modeled with regions defined based on summer conditions and winter processes modeled using winter-based

regions, such as SWE regimes. Furthermore, by integrating the two time periods, we may be better able to represent processes that occur annually, and understand the temporal dynamics of many physical processes for which a yearly perspective is required.

While we have demonstrated the current analysis using spatial–temporal data on SWE, this analysis also has implications for other types of spatial–temporal analysis in the natural and human environments where data are collected at fine temporal resolutions over long time periods. In this research we have defined and presented a suite of metrics representative of a range of temporal dynamics of SWE accumulation and depletion processes. Further, we have demonstrated an aggregation approach for integrating metrics to provide insights (both quantitatively and visually) on the multi-temporal trends exhibited. Additional opportunities for applying the metrics and logic presented in this research are possible where appropriate datasets are available, such as in the delineation of animal home-ranges, identification of soil and atmospheric regimes, assessing change and delineating housing markets, as well to derive estimates of representative scales for general spatial analysis.

References

Armstrong, R., & Brodzik, M. (1995). An earth-gridded SSM/I data set for cryospheric studies and global change monitoring. *Advanced Space Research*, 16, 10155−10163.

Armstrong, R., Knowles, K., Brodzik, M., Hardman, M., et al. (2002). *1994–2002. DMSP SSM/I Pathfinder daily EASE-Grid brightness temperatures. Boulder, CO, National Snow and Ice Data Center. Digital media and CD-ROM.*

Bailey, N. T. J. (1985). The role of statistics in controlling and eradicating infectious diseases. *The Statistician*, 34, 3−17.

Barnett, T. P., Adam, J. C., Lettenmaie, D. P., et al. (2005). Potential impacts of a warming climate on water availability in snow-dominated regions. *Nature*, 438, 303−309.

Blasi, C., Carranza, M. L., Frondoni, R., Rosati, L., et al. (2000). Ecosystem classification and mapping: A proposal for Italian landscapes. *Applied Vegetation Science*, 3, 233−242.

Bradley, B. A., Jacob, R. W., Hermance, J. F., Mustard, J. F., et al. (2007). A curve fitting procedure to derive inter-annual phenologies from time series of noisy satellite NDVI data. *Remote Sensing of Environment*, 106, 137−145.

Brown, R. (2000). Northern Hemisphere snow cover variability and change, 1915–1997. *Journal of Climate*, 13, 2339−2355.

Chang, A. T. C., Kelly, R. E. J., Foster, J. L., et al., & Hall, D. K. (2003). Global SWE monitoring using AMSR-E data. *Geoscience and Remote Sensing Symposium, 2003. IGARSS '03 Proceedings. 2003 IEEE International*, Vol. 1. (pp. 680−682).

Craven, P., & Wahba, G. (1979). Smoothing noisy data with spline functions: Estimating the correct degree of smoothing by the method of generalized cross-validation. *Numerical Mathematics*, 31(4), 377−403.

Coops, N. C., Wulder, M. A., Duro, D. C., Han, T., Berry, S., et al. (2008). *Ecological Indicators*, 8, 754−766.

DeFries, R., Hansen, M., Townshend, J., et al. (1995). Global discrimination of land cover types from metrics derived from AVHRR Pathfinder data. *Remote Sensing of Environment*, 54, 209−222.

Derksen, C., & McKay, M. (2006). The Canadian boreal snow water equivalent band. *Atmosphere-Ocean*, 44, 305−320.

Derksen, C., Walker, A., Goodison, B., et al. (2003). A comparison of 18 winter seasons of in situ and passive microwave derived snow water equivalent estimates in Western Canada. *Remote Sensing of Environment*, 88, 271−282.

Derksen, C., Walker, D. A., Ledrew, E., Goodison, B., et al. (2002). Time-series analysis of passive-microwave-derived central North American snow water equivalent imagery. *Annals of Glaciology*, 34, 1−7.

Derksen, C., LeDrew, E., Goodison, B., et al. (1998). SSM/I derived snow water equivalent data: The potential for investigating linkages between snow cover and atmospheric circulation. *Atmosphere-Ocean*, 36, 95−117.

Derksen, C., LeDrew, E., Goodison, B., et al. (1998). Application of the Getis statistic to hemispheric and regional scale passive microwave derived snow water equivalent imagery. *Geoscience and Remote Sensing Symposium Proceedings IGARSS '98. 1998 IEEE International*, Vol. 2. (pp. 977−979).

Derksen, C., LeDrew, E., Goodison, B., et al. (2000). Temporal and spatial variability of North American prairie snow cover (1988–1995) inferred from passive micro-wave-derived snow water equivalent imagery. *Water Resources Research*, 36, 255−266.

Derksen, C., Walker, A., Goodison, B., et al. (2005). Evaluation of passive microwave snow water equivalent retrievals across the boreal forest/tundra transition of western Canada. *Remote Sensing of Environment*, *96*, 315–327.

Derksen, C., LeDrew, E., Walker, A., Goodison, B., et al. (2000). Winter season variability in North American prairie SWE distribution and atmospheric circulation. *57th Eastern Snow Conference, Syracuse, New York, USA*.

Derksen, C., Wulder, M. A., LeDrew, E., Goodison, B., et al. (1998). Associations between spatially autocorrelated patterns of SSM/I derived Prairie snow cover and atmospheric circulation. *Hydrological Processes*, *12*, 2307–2316.

Duro, D. C., Coops, N. C., Wulder, M. A., Han, T., et al. (2007). Development of a large area biodiversity monitoring system driven by remote sensing. *Progress in Physical Geography*, *31*, 235–260.

Efron, B. (1979). Bootstrap methods: Another look at the jackknife. *Annals of Statistics*, *7*, 1–26.

Efron, B., Halloran, E., Holmes, S., et al. (1996). Bootstrap confidence levels for phylogenetic trees. *Proceedings of the National Academy of Sciences*, *93*, 13429.

Ellis, D. V., Samoszynski, R., Jones, A. A., et al. (1991). Re-analysis of species associational data using bootstrap significance tests. *Water, Air, & Soil Pollution*, *59*, 347–358.

Everitt, B. S. (1974). *Cluster analysis*. London: Heinemann.

Felsenstein, J. (1985). Confidence limits on phylogenies: An approach using the bootstrap. *Evolution*, *39*, 783–791.

Foster, J., Hall, D., Chang, A., Rango, A., Wergin, W., Erbe, E., et al. (1999). Effects of snow crystal shape on the scattering of passive microwave radiation. *IEEE Transactions on Geoscience and Remote Sensing*, *37*, 1165–1168.

Fovell, Robert G., & Fovell, Mei-Ying C. (1993). Climate zones of the conterminous United States defined using cluster analysis. *Journal of Climate*, *6*, 2103–2135.

Goita, K., Walker, A. E., & Goodison, B. E. (2003). Algorithm development for the estimation of snow water equivalent in the boreal forest using passive microwave data. *International Journal of Remote Sensing*, *24*, 1097–1102.

Gong, X., & Richman, M. B. (1995). On the application of cluster analysis to growing season precipitation data in North America east of the Rockies. *Journal of Climate*, *8*, 897–931.

Goodison, B. (1989). Determination of areal snow water equivalent on the Canadian Prairies using passive microwave satellite data. *Geoscience and Remote Sensing Symposium, 1989. IGARSS'8912th Canadian Symposium on Remote Sensing, Vol. 3*. (pp. 1243–1246).

Goodison, B., & Walker, A. (1995). Canadian development and use of snow cover information from passive microwave satellite data. In B. Choudhury, Y. Kerr, E. Njoku & P. Pampaloni (Eds.), *Passive microwave remote sensing of land–atmosphere interactions* (pp. 245–262). Utrecht, Netherlands: VSP BV.

Green, P. J., & Silverman, B. W. (1994). *Nonparametric regression and generalized linear models: A roughness penalty approach*. Chapman & Hall/CRC.

Grody, N. C., & Basist, A. N. (1996). Global identification of snowcover using SSM/I measurements. *IEEE Transactions on Geoscience and Remote Sensing, 34*, 237–249.

Hennig, C. (2007). Cluster-wise assessment of cluster stability. *Computational statistics and data analysis*, *52*, 258–271.

Hermance, J. F., Jacob, R. W., Bradley, B. A., Mustard, J. F., et al. (2007). Extracting phenological signals from multiyear AVHRR NDVI time series: Framework for applying high-order annual splines with roughness damping. *IEEE Transactions on Geoscience and Remote Sensing*, *45*, 3264–3276.

Hermance, J. F. (2007). Stabilizing high-order, non-classical harmonic analysis of NDVI data for average annual models by damping model roughness. *International Journal of Remote Sensing*, *28*, 2801–2819.

Hirsch, A., Cushwa, C. T., Flach, K. W., Frayer, W. E., et al. (1978). Land classification — Where do we go from here? *Journal of Forestry*, *76*, 672–673.

Ironside, G. R. (1991). Ecological land survey: Background and general approach. *Guidelines for the integration of wildlife and habitat evaluations with ecological land survey. Wildlife Habitat Canada and Environment, Vol. 107*. Ottawa, ON: Canada, Canadian Wildlife Service.

Jaccard, P. (1901). Distribution de la flore alpine dans le bassin des dranses et dans quelque region vasines. *Bulletin de la Societe Vaudoise des Sciences Naturelles*, *37*, 241–272.

Johnston, J. W. (1976). *Similarity indices I: What do they measure*. Richland, WA, USA: Battelle Pacific Northwest Labs.

Justice, C. O., Townshend, J. R. G., Holben, B. N., Tucker, C. J., et al. (1985). Analysis of the phenology of global vegetation using meteorological satellite data. *International Journal of Remote Sensing*, *6*, 1271–1318.

Karl, T. R., Jones, P. D., Knight, R. W., Kukla, G., Plummer, N., Razuvayev, V., et al. (1993). A new perspective on recent global warming: Asymmetric trends of daily maximum and minimum temperature. *Bulletin of the American Meteorological Society*, *74*, 1007–1023.

Kaufman, L., & Rousseeuw, P. J. (1990). *Finding groups in data*. New York: Wiley.

Kerr, M. Kathleen, & Churchill, Gary A. (2001). Bootstrapping cluster analysis: Assessing the reliability of conclusions from microarray experiments. *Proceedings of the National Academy of Sciences*, *98*, 8961–8965.

Knowles, K., Njoku, E., Armstrong, R., Brodzik, M., et al. (1999). *Nimbus-7 SMMR Pathfinder daily EASE-Grid brightness temperatures. Boulder, CO: National Snow and Ice Data Center. Digital media and CD-ROM*.

Kudo, G. (1991). Effects of snow-free period on the phenology of alpine plants inhabiting snow patches. *Arctic and Alpine Research*, *23*, 436–443.

Laternser, M., & Schneebeli, M. (2003). Long-term snow climate trends of the Swiss Alps (1931–1999). *International Journal of Climatology*, *23*, 733–750.

Lloyd, D. (1990). A phenological classification of terrestrial vegetation cover using shortwave vegetation index imagery. *International Journal of Remote Sensing*, *11*, 2269–2279.

Luce, C., Tarboton, D., & Cooley, K. (1998). The influence of the spatial distribution of snow on basin-average snow melt. *Hydrological Processes*, *12*, 1671–1683.

MacKay, M. D., Seglenieks, F., Verseghy, D., Soulis, E. D., Snelgrove, K. R., Walker, A., et al. (2003). Modeling Mackenzie Basin Surface Water Balance during CAGES with the Canadian Regional Climate Model. *Journal of Hydrometeorology*, *4*, 748–767.

Malingreau, J. P. (1986). Global vegetation dynamics: Satellite observations over Asia. *International Journal of Remote Sensing*, *7*, 1121–1146.

Marshall, I. B., Wiken, E. B., Hirvonen, H., et al. (1998). *Terrestrial Ecoprovinces of Canada. Ecosystem Sciences Directorate, Environment Canada and Research Branch*. Ottawa/Hull: Agriculture and Agri-Food Canada.

Mccarty, John P. (2001). Ecological consequences of recent climate change. *Conservation Biology*, *15*.

McKenna, J. E. (2001). Biological structure and dynamics of littoral fish assemblages in the Eastern Finger Lakes. *Aquatic Ecosystem Health & Management*, *4*, 91–114.

Mckenna, J. E. (2003). An enhanced cluster analysis program with bootstrap significance testing for ecological community analysis. *Environmental Modelling and Software*, *18*, 205–220.

Milligan, G. W., & Cooper, M. C. (1985). An examination of procedures for determining the number of clusters in a data set. *Psychometrika*, *50*, 159–179.

Moody, A., & Johnson, D. M. (2001). Land-surface phenologies from AVHRR using the discrete Fourier transform. *Remote Sensing of Environment*, *75*, 305–323.

Moulin, S., Kergoat, L., Viovy, N., Dedieu, G., et al. (1997). Global-scale assessment of vegetation phenology using NOAA/AVHRR satellite measurements. *Journal of Climate*, *10*, 1154–1170.

Nemec, A. F. L., & Brinkhurst, R. O. (1988). Using the bootstrap to assess statistical significance in the cluster analysis of species abundance data. *Canadian Journal of Fisheries and Aquatic Sciences*, *45*, 965–970.

Pillar, V. D. P. (1999). How sharp are classifications? *Ecology*, *80*, 2508–2516.

Poff, N. (1996). A hydrogeography of unregulated streams in the United States and an examination of scale-dependence in some hydrological descriptors. *Freshwater Biology*, *36*, 71–79.

Pulliainen, J., & Halliskainen, M. (2001). Retrieval of regional snow water equivalent from space-borne passive microwave observations. *Remote Sensing of Environment*, *75*, 76–85.

Rao, A. R., & Srinivas, V. V. (2006). Regionalization of watersheds by hybrid-cluster analysis. *Journal of Hydrology*, *318*, 37–56.

Reed, B. C., Brown, J. F., VanderZee, D., Loveland, T. R., et al. (1994). Measuring phenological variability from satellite imagery. *Journal of Vegetation Science*, *5*, 703–714.

Rowe, J. S., & Sheard, J. W. (1981). Ecological land classification: A survey approach. *Environmental Management*, *5*, 451–464.

Serreze, M., Walsh, J., Chapin, F., Osterkamp, T., Dyurgerov, M., Romanosky, V., et al. (2000). Observational evidence of recent change in the northern high-latitude environment. *Climatic Change*, *46*, 159–207.

Sims, R. A., Corns, I. G. W., Klinka, K., et al. (1996). Global to local: Ecological land classification. *Environmental Monitoring and Assessment*, *39*, 1–10.

Smith, S. P., & Dubes, R. (1980). Stability of a hierarchical clustering. *Pattern Recognition*, *12*, 177–187.

Sneath, P. H. A., & Sokal, R. R. (1973). *Numerical taxonomy: The principles and practice of numerical classification*. San Francisco, USA: WH Freeman & Co.

Sokol, J., Pultz, T. J., Walker, A. E., et al. (2003). Passive and active airborne microwave remote sensing of snow cover. *International Journal of Remote Sensing*, *24*, 5327–5344.

Sturm, M., Holmgren, J., Liston, G. E., et al. (1995). A seasonal snow cover classification system for local to global applications. *Journal of Climate*, *8*, 1261–1283.

Tait, A. (1996). Estimation of snow water equivalent using passive microwave radiation data *Proceedings of the IEEE 2000 International Geoscience and Remote Sensing Symposium, 4*. (pp. 2005–2007).

Unal, Y., Kindap, T., Karaca, M., et al. (2003). Redefining the climate zones of Turkey using cluster analysis. *International Journal of Climatology*, *23*, 1045–1055.

Walker, A. E., & Silis, A. (2002). Snow-cover variations over the Mackenzie River basin, Canada, derived from SSM/I passive-microwave satellite data. *Annals of Glaciology*, *34*, 8–14.

Walker, A., & Goodison, B. (2000). Challenges in determining snow water equivalent over Canada using microwave radiometry. *Proceedings of the IEEE 2000 International Geoscience and Remote Sensing Symposium, Vol. 4*. (pp. 1551–1554).

Walker, D. A., Halfpenny, J. C., Walker, M. D., Wessman, C. A., et al. (1993). Long-term studies of snow–vegetation interactions. *BioScience*, *43*, 287–301.

Walker, M. D., Walker, D. A., Welker, J. M., Arft, A. M., Bardsley, T., Brooks, P. D., et al. (1999). Long-term experimental manipulation of winter snow regime and summer temperature in arctic and alpine tundra. *Hydrological Processes*, *13*, 2315–2330.

Walther, G. -R., Post, E., Convey, P., Menzel, A., Parmesan, C., Beebee, T. J. C., et al. (2002). Ecological responses to recent climate change. *Nature*, *416*, 389–395.

Wiken, E. B. (1986). *Terrestrial ecozones of Canada. Ecological land classification*. Environment Canada.

Wiken, E., Gauthier, D., Marshall, I., Lawton, K., Hirvonen, H., et al. (1996). *A perspective on Canada's ecosystems, Occasional Paper No. 14*. Ottawa, ON, Canada: Canadian Council on Ecological Areas.

Wulder, M. A., Nelson, T., Derksen, C., Seemann, D., et al. (2007). Snow cover variability across central Canada (1978–2002) derived from satellite passive microwave data. *Climatic Change*, *82*, 113–130.